HHS Public Access

Author manuscript

Nat Immunol. Author manuscript; available in PMC 2026 January 27.

Published in final edited form as:

Nat Immunol. 2019 April ; 20(4): 420–432. doi:10.1038/s41590-019-0336-y.

NAD+ salvage dependence due to ROS-mediated DNA damage in inflammatory macrophages

Alanna M. Cameron[1], **Angela Castoldi**[1], **David E. Sanin**[1], **Lea J. Flachsmann**[1], **Cameron S. Field**[1], **Daniel. J. Puleston**[1,2], **Ryan L. Kyle**[1], **Annette E. Patterson**[1], **Fabian Hässler**[1], **Joerg M. Buescher**[1], **Beth Kelly**[1], **Erika L. Pearce**[1], **Edward J. Pearce**[1,3,*]

[1]Department of Immunometabolism, Max Planck Institute of Immunobiology and Epigenetics, Freiburg im Breisgau, Germany.

[2]The Kennedy Institute of Rheumatology, University of Oxford, Oxford, UK

[3]Faculty of Biology, University of Freiburg, Freiburg im Breisgau, Germany

Abstract

Adoption of Warburg metabolism is critical for macrophage activation in response to lipopolysaccharide (LPS). Macrophages stimulated with LPS increase expression of nicotinamide phosphoribosyltransferase (NAMPT), a key enzyme in NAD^+ salvage, and loss of NAMPT activity alters their inflammatory potential. However, events leading to NAD^+ salvage-dependence in these cells remain poorly defined. We show that NAD^+ depletion and increased NAMPT expression occurred rapidly after inflammatory activation and coincided with DNA damage caused by reactive oxygen species (ROS). ROS produced by Complex III of the mitochondrial electron transport chain was required for macrophage activation. DNA damage was associated with poly-ADP-ribose polymerase (PARP) activation, which results in NAD^+ consumption. In this setting increased NAMPT expression allowed for the maintenance of NAD^+ pools sufficient for glyceraldehyde-3-phosphate dehydrogenase (GAPDH) activity and Warburg metabolism. Our findings provide an integrated explanation for dependency on the NAD^+ salvage pathway in inflammatory macrophages.

Introduction

Macrophages are resident in mammalian tissues, and are capable of becoming differentially activated in response to changing conditions and adopting functions that allow them to fight infection, and support tissue homeostasis[1]. Recent work showed that receptor systems that mediate macrophage activation are linked to metabolic pathways, and that

*Correspondence: pearceed@ie-freiburg.mpg.de.

Author contributions

A.M.C., A.C., B.K., E.L.P. and E.J.P. designed experiments and provided conceptual input. A.M.C., A.C., L.J.F., C.S.F., D.J.P., R.L.K., A.E.P, F.H. and J.M.B., performed experiments and developed methodologies. A.M.C., A.C., L.J.F., D.E.S., E.L.P. and E.J.P. analyzed data. A.M.C. and E.J.P. wrote the manuscript.

Declaration of interests

E.J.P. and E.L.P. are founders of Rheos Medicines. E.L.P. is a member of the SAB for ImmunoMet Therapeutics.

metabolic reprogramming is integral to activation[2, 3, 4, 5, 6, 7]. Redox balance is a critical aspect of these processes, as cells must sustain metabolic events that require NADH and NAD^+ (for example, the fueling of the electron transport chain, ETC, and the activity of the glycolysis enzyme glyceraldehyde-3-phosphate dehydrogenase, GAPDH, respectively). While cells have intrinsic mechanisms to balance redox between mitochondria and cytoplasm through the use of mitochondrial shuttles[8], these processes can become unbalanced when NAD^+ is depleted by NAD^+-consuming enzymes such as poly- ADP-ribose polymerases (PARPs), sirtuins and CD38[9]. In this situation the NAD^+ salvage pathway can assume a critical role, recycling nicotinamide, the byproduct of NAD^+ consuming enzymes, into nicotinamide mononucleotide (NMN), which is then converted to NAD^+[9]. Increased expression of nicotinamide phosphoribosyltransferase (NAMPT), the rate-limiting enzyme in the NAD^+ salvage pathway, has been reported in macrophages activated by LPS with or without interferon-γ (IFN-γ)[10, 11, 12, 13]; implying an underlying redox imbalance during inflammation[14]. We were interested in investigating causes and consequences of this situation, and in examining whether this was also the case in the contrasting alternative activation state induced by IL-4.

Our data indicate that stimulation with LPS or IFN-γ and LPS (γ+LPS) led to an NAD^+ imbalance linked to a rapid, extensive DNA damage response and PARP activation. This was accompanied by the upregulation of the NAD^+ salvage pathway, which was critical for the cells to sustain Warburg metabolism linked to cellular activation by LPS. We found that the initiator of the DNA damage response in these cells is a stimulus-linked increase in mitochondrial ROS production at ETC Complex III (CIII), a process that itself is required for inflammatory activation.

Results

Inflammatory macrophages depend on NAD^+ salvage

Previous reports have linked expression of *Nampt* to inflammatory states in which macrophages are implicated[10, 11, 12, 13, 15]. We were interested in why NAMPT would be expressed in inflammatory macrophages. To explore this we measured NAD^+ in bone marrow-derived C57BL/6J mouse macrophages stimulated with γ+LPS or LPS for 18 h. Compared to resting macrophages (M0), or IL-4-stimulated macrophages (M(IL-4)), NAD^+ was significantly decreased in M(γ+LPS) and M(LPS) (Fig. 1a, Supplementary Fig. 1a). Decreases in NAD^+ in inflammatory macrophages were accompanied by lower NADH, $NADP^+$ and NADPH levels, indicating an overall decline in the NAD pool[14] (Fig. 1b, Supplementary Fig. 1b). Diminished NAD^+ correlated with increased expression of *Nampt* and genes encoding other enzymes in the pathway, such as *Nmnat1* (Fig. 1c, d, Supplementary Fig. 1c), while expression of genes encoding key enzymes in the Preiss-Handler pathway for NAD^+ synthesis from vitamin B3 and the de novo biosynthesis pathway remained unchanged (Supplementary Fig. 1d). Thus, increased *Nampt* expression correlated with diminished NAD^+ in inflammatory macrophages, suggesting that NAD^+ salvage was engaged to maintain sufficient NAD^+ for cellular functions. To examine this, we treated macrophages with FK866 (APO866), a specific inhibitor of NAMPT[16] (Fig. 1e). This drug led to the depletion of NAD^+ and NADH in M(γ+LPS) and M(LPS), but

also to decreases in M0 and M(IL-4) (Fig. 1f, Supplementary Fig. 1e). Consistent with the importance of NAD^+ salvage in inflammatory macrophages, FK866 treatment induced dose-dependent cell death in M(γ+LPS) and M(LPS) (Fig. 1g, Supplementary Fig. 1f). M0 and M(IL-4) viability was affected to a lesser extent by FK866 (Fig. 1g). In C57BL/6J mice the gene encoding NAD nucleotide transhydrogenase (Nnt) is mutated, resulting in reduced Nnt activity, which can manifest in redox-related imbalances[17]. However, diminished NAD^+ levels in M(γ+LPS) and M(LPS) were also observed in C57BL/6N macrophages, which possess functional Nnt, and the NAD^+ pool in these cells was sensitive to NAMPT inhibition (Supplementary Fig. 1g). Collectively, these results suggest that M(γ+LPS) and M(LPS) rely on NAMPT to maintain NAD^+ pools that are compatible with survival, while M0 and M(IL-4) utilize, but are less dependent on, NAD^+ salvage.

Inflammatory macrophages need NAD^+ for Warburg metabolism

To examine differing NAMPT requirements in macrophages of distinct polarization states, we asked how NAMPT inhibition affects macrophage metabolism. We measured the extracellular acidification rate (ECAR) indicative of aerobic glycolysis, and oxygen consumption rate (OCR) as a readout of oxidative phosphorylation (OXPHOS), in M0, M(γ+LPS), M(LPS) and M(IL-4) stimulated for 18 h in the presence or absence of FK866 (Fig. 2a-d). FK866 had little effect on ECAR or OCR in M0 macrophages, even under conditions in which OXPHOS was inhibited (by the addition of oligomycin), or when oxygen consumption was uncoupled from ATP production by FCCP (Fig. 2a). However, the ability of M(γ+LPS) and M(LPS) to increase ECAR in response to the addition of glucose was inhibited by FK866 (Fig. 2b,c, Supplementary Fig. 2a,b), which correlated with decreased extracellular lactate (Supplementary Fig. 2c,d), suggesting a link between NAD^+ salvage and glycolytic metabolism in these cells. As expected[18], M(γ+LPS) did not have measurable OXPHOS, and OCR was unaffected by NAMPT inhibition (Fig. 2b, Supplementary Fig. 2e). However, in M(LPS) OCR was inhibited by FK866 treatment (Fig. 2c, Supplementary Fig. 2f). Consistent with the susceptibility of M(γ+LPS) and M(LPS) to NAMPT inhibition, and the importance of Warburg metabolism in these cells[7], FK866 treatment resulted in reduced cellular ATP (Fig. 2f,g). Treatment of M(γ+LPS) with additional NAMPT inhibitors, GPP78 and STF118804, mirrored the metabolic effects observed with FK866 (Supplementary Fig. 2g-j). In contrast, glycolysis and OXPHOS in M(IL-4) were unaffected by treatment with FK866, and the ATP pool in these cells, and in M0, remained unchanged after NAMPT inhibition (Fig. 2a,d,e,h).

We next attempted to identify mechanisms underlying reduced glycolysis associated with NAMPT inhibition in inflammatory macrophages. Transcriptional analyses revealed mostly increased expression of glycolytic genes in M(γ+LPS) and M(LPS) cells upon FK866 treatment (Supplementary Fig. 2k,l). Thus, we reasoned that the decrease in glycolytic rate might reflect diminished activity of GAPDH due to limiting NAD^+[19]. Measurements of glycolysis pathway metabolites were consistent with this, revealing the accumulation of intermediates upstream of GAPDH, and decreases in downstream intermediates in FK866-treated M(γ+LPS)and M(LPS) (Fig. 2i, j, Supplementary Fig. 2m). Moreover, treatment of M(γ+LPS) and M(LPS) with the selective GAPDH inhibitor heptelidic acid (HA)[20], affected the metabolic profile of these cells similarly to FK866 treatment (Supplementary

Fig. 2n-q). OCR of M(LPS) was also diminished with HA, supporting the idea that OXPHOS is affected in M(LPS) when glycolytic rate is reduced (Supplementary Fig. 2p). These data reinforce the view that, in inflammatory macrophages, the GAPDH demand for NAD^+ is being met by NAD^+ salvage, although it is also possible that NAD^+ and NADH depletion due to NAMPT inhibition could be directly affecting TCA cycle and ETC functions. To confirm the specificity of the effects of FK866, we utilized shRNA to reduce NAMPT expression (Supplementary Fig. 2r). *Nampt*-shRNA-treated macrophages stimulated with γ+LPS did not lose viability after polarization, but exhibited similar metabolic defects to NAMPT inhibitor-treated M(γ+LPS), having a lower glycolytic rate and NAD^+ pool than cells transduced with an empty vector (Fig. 2k,l,m). Together, these data indicate that NAMPT is important for the characteristic metabolic program of inflammatory macrophages.

NAMPT modulates inflammatory macrophage activation

Given the dependence of inflammatory macrophage activation on Warburg metabolism and the importance of NAMPT for this process, we reasoned FK866 would inhibit γ+LPS and LPS-induced cellular activation. Consistent with this, we found that FK866 significantly impaired expression of activation markers including CD80, NOS2, pro-IL-1β, IL-6 and tumor necrosis factor (TNF) *in vitro* (Fig. 3a-e, Supplementary Fig. 3a,b). Unbiased measurements of transcriptional changes using RNA-seq revealed corresponding changes only in *Cd80* and *Tnf*, suggesting that much of the observed regulation may occur post-transcriptionally (Supplementary Fig. 3c). Nevertheless, FK866 treatment had broad positive in addition to negative effects on the expression of genes encoding other inflammatory mediators (Fig. 3f). For example, FK866 diminished the expression of *Ccl3, Ccl7, Cxcl10, Ifna1* and *Tnfsf10* but also enhanced expression of *Ccl6*, *Ccl9, Ccl22, Tnfsf15* and *Il12b* (Fig. 3f). While *Il12b* mRNA was significantly increased in FK866-treated M(γ+LPS), production of IL-12 remained unchanged (Fig. 3g, Supplementary Fig. 3c). In contrast, surface MHC II expression was increased by FK866 treatment despite a lack of transcriptional change (Fig. 3h, Supplementary Fig. 3c). Similar effects on viability, CD80, NOS2 and MHC II expression were observed when M(γ+LPS) were treated with GPP78 and STF118804 (Fig. Supplementary Fig. 3d,e). Inhibition of GAPDH by HA had similar effects on NOS2 expression and IL-6 and TNF production (Supplementary Fig. 3f), supporting the view that the impact of NAMPT inhibition on these parameters reflects decreased GAPDH activity. Expression of RELMα, CD206 and CD301 by M(IL-4) was unaffected by FK866 (Supplementary Fig. 3g). The importance of NAMPT for inflammatory macrophage activation was confirmed by analysis of *Nampt*-shRNA-treated M(γ+LPS) macrophages, which expressed less NOS2, IL-6 and TNF, and more MHC II when compared to control cells (Fig. 3i-l). These data collectively support the view that NAD^+ salvage is required for inflammatory but not alternative macrophage activation.

We found that FK866 treatment of mice with LPS-induced systemic inflammation diminished disease severity, measured as the hypothermic response to LPS injection (Fig. 4a) and lowered concentrations of LPS-induced serum IL-1β, TNF and IL-6 (Fig. 4b–d). This was not accompanied by significant changes in macrophage frequency within the peritoneal lavage. As expected[21], LPS alone decreased the recovery of peritoneal

macrophages (pMacs); despite this, frequencies of total macrophages, Tim4^{+} resident and Tim4^{-} infiltrating pMacs were not further impacted by FK866 treatment (Fig. 4e-g). Frequencies of other pro-inflammatory cytokine producing immune cells, such as eosinophils, neutrophils and dendritic cells (DCs) were also unaffected by FK866 treatment (Supplementary Fig. 4a-c). We found that pMacs from LPS-injected mice exhibited increased ECAR and OCR similar to that observed in LPS-stimulated bone marrow derived macrophages, which again was susceptible to FK866 inhibition (Fig. 4h,i, Supplementary Fig. 4d). LPS-stimulated changes in metabolism, and inhibitory effects of FK866 thereon, were also apparent in epididymal fat macrophages (Supplementary Fig. 4e). As observed in peritoneal cells, FK866 did not cause significant alterations in LPS-induced effects on the immune cell frequency of the adipose tissue (Supplementary Fig. 4f-i). Together, these data suggest that *in vivo* anti-inflammatory effects of FK866 treatment are likely a direct result of modulation of the core metabolic program of inflammatory macrophages.

NMN rescues FK866-induced activation defects

NMN is the metabolite directly downstream of NAMPT in the NAD^{+} salvage pathway (Fig. 1e). Supplementation with NMN resulted in significant recovery of glycolysis and ATP in FK866-treated M(γ+LPS) (Fig. 5a-c). This was accompanied by a reduction in accumulated glucose-6-phosphate and fructose-6-phosphate upstream of GAPDH and an increase in 2-phosphoglycerate and 3-phosphoglycerate downstream of GAPDH (Fig. 5d), supporting the view that NMN supplementation allows some recovery of GAPDH function. Consistent with this, NMN increased, although did not fully restore, NAD^{+} levels (Fig. 5e). The rescue of metabolic defects by the addition of NMN was accompanied by an improvement in viability (Fig. 5f) and reversal of FK866-mediated effects on CD80, NOS2, MHCII, IL-6 and TNF expression (Fig. 5g,h). In contrast, supplementation with pyruvate was unable to restore the metabolic effects, or rescue decreased viability and phenotypic defects associated with FK866 treatment (Supplementary Fig. 5a-f). These data support the view that NAMPT inhibitor effects on inflammatory macrophages are due to disruption of the NAD^{+} salvage pathway.

DNA damage leads to NAD^{+} depletion

The critical role for NAD^{+} salvage in inflammatory macrophages prompted us to examine the events that lead to NAD^{+} depletion. We examined NAD^{+} over time, and found a decline was apparent as early as 1 h post-activation in M(γ+LPS) and M(LPS) (Fig. 6a,b). This was reflected in lower NAD^{+} and NADH in these cells, compared to generally higher NAD^{+} and NADH in M0 and M(IL-4) (Fig. 6b,c; Supplementary Fig. 6a). Similar trends were observed with NADPH, which was decreased in M(γ+LPS) after 1 h of activation, although NADP^{+} levels remained unchanged in macrophages of all polarization states at this time point (Supplementary Fig. 6a). A transcriptional response to this NAD^{+} imbalance was already apparent at this early juncture, with *Nampt* mRNA, although not protein, significantly upregulated in M(γ+LPS) (Fig. 6d; Supplementary Fig. 6b,c) and NAD^{+} levels were already sensitive to FK866 (Fig. 6e). These data imply that NAD^{+} is rapidly consumed once inflammatory macrophage activation is initiated. Among major NAD^{+} consuming systems, we found CD38 was expressed by M(γ+LPS) or M(LPS) only later during activation (Supplementary Fig. 6d). However, PARPs are expressed in resting macrophages, and we

measured significantly increased expression of PARPs 3, 4, 9, 10 and 12 in M(γ+LPS) at 1 h post-activation (Fig. Supplementary 6e). This transcriptional response was consolidated thereafter, and also apparent in M(LPS) at 18 h (Supplementary Fig. 6f). Further analysis revealed evidence of a transcriptional DNA damage signature, with strong enrichment in expression of DNA damage response-associated genes in M(γ+LPS) and M(LPS) compared to M0, or M(IL-4) at 1 h post-activation (Fig. 6f, Supplementary Fig. 6g). We found a strong signal for γ-H2AX, a mark of DNA damage, in the majority of macrophages at 1 h and 18 h post-stimulation with γ+LPS or LPS alone but not in resting or IL-4 activated macrophages (Fig. 6g,h). Increased γ-H2AX was additionally detected *ex vivo* in pMacs isolated 1 h after i.p. LPS injection (Fig. 6i). The decreases in NAD^+ and accumulation of DNA damage observed in C57BL/6J macrophages at 1 h after γ+LPS and LPS stimulation were seen in macrophages with functional NNT (Supplementary Fig. 6h,i).

We reasoned that PARP activation in response to DNA damage could account for NAD^+ depletion. Consistent with this, increased PARP activity, measured as amount of PAR in cell extracts, was evident after 1 h of γ+LPS or LPS stimulation (Fig. 6j). To further examine this we used the PARP inhibitor Rucaparib[22], which markedly decreased total cellular PAR levels (Fig. 6k). Rucaparib treatment resulted in increased NAD^+ in M(γ+LPS) (Fig. 6l). Furthermore, inhibition of PARPs resulted in significantly increased DNA damage in M(γ+LPS), which was associated with a dose-dependent decrease in viability (Fig. 6m; Supplementary Fig. 6j). In addition, PARP inhibition altered the polarization of M(γ+LPS), with Rucaparib treatment decreasing expression of CD80 and NOS2, and IL-6 production, while MHC II expression and TNF production were unaffected (Supplementary Fig. 6k, l). Increased DNA damage was also apparent in M(LPS), but not M0 or M(IL-4), following Rucaparib treatment (Supplementary Fig. 6m-o). Thus, NAD^+ depletion is likely to be a reflection of increased PARP activation occurring in response to early onset DNA damage in M(γ+LPS) or M(LPS). We next examined if PARP inhibition would abrogate the metabolic requirement of M(γ+LPS) for NAD^+ salvage. We found that PARP inhibitors alone had no effect on the ECAR of M(γ+LPS), however combined PARP and NAMPT inhibition resulted in less significant decreases in glycolysis than NAMPT inhibition alone (Fig. 6n, Supplementary Fig. 6p). These results support the conclusion that PARP-mediated depletion of NAD^+ is a major event driving M(γ+LPS) dependency on NAMPT.

Mitochondrial ROS is responsible for DNA damage

At late times post activation with γ+LPS or LPS, nitric oxide (NO) has been shown to be an important mediator of DNA damage [23, 24]. However, we observed γ-H2AX staining preceding the onset of NO production (Supplementary Fig. 7a). In this context, we reasoned the most likely candidate to cause DNA damage was ROS. This was supported by significant, rapid (within 1 h) increases in the expression of oxidative stress response genes in M(γ+LPS) compared to M0 (Fig. 7a). This early signature included increased expression of *Nfe2l2*, which encodes the transcription factor Nrf2, which itself activates transcriptional anti-oxidant responses, as well as decreased expression of *Keap1*, which encodes a negative regulator of Nrf2 (Fig. 7a)[25]. This was associated with increased levels of Nrf2 protein in M(γ+LPS) after 1 h of activation, which was further increased and also evident in M(LPS) by 18 h of activation (Supplementary Fig. 7b).

ROS can be produced during respiration, but also in phagocytic immune cells by NADPH oxidase, which is activated in LPS-stimulated macrophages within the time frame of interest here[26]. We found that 1 h after activation, DNA damage was equivalent in γ+LPS or LPS-activated wild-type and *Cybb*$^{-/-}$ macrophages, which lack the functionally critical gp91^{phox} component of NADPH oxidase (Fig. 7b). We next examined whether mitochondria could be contributing ROS to cause DNA damage. We found the basal OCR of M(γ+LPS) and M(LPS) was increased between 0.5 and 1 h post-activation (Fig. 7c,d, Supplementary Fig. 7c,d). This was paralleled by a transient increase in spare respiratory capacity (SRC), which dissipated by 4 h (Fig. 7e, Supplementary Fig. 7e). In parallel with increased respiration, we measured an activation-induced increase in mitochondria-produced ROS as measured by MitoSOX staining (Fig. 7f). We found that treatment with N-acetylcysteine (NAC), which can directly scavenge ROS and promote ROS detoxification[27, 28], or the mitochondria-specific ROS scavenger MitoTempol, decreased the magnitude of both mitochondrial ROS production and γ-H2AX marked DNA damage (Fig. 7 g-j, Supplementary Fig. 7f-h). As an independent measure of oxidative DNA damage we stained cells for 8-hydroxyguanosine (8OHG). We observed a strong 8OHG signal at 1 h post stimulation with M(γ+LPS) or M(LPS), but not in M(0) or M(IL-4) (Fig. 7k, Supplementary Fig. 7i). 8OHG staining was apparent in nuclei, but also as punctate foci throughout the cytoplasm (Fig. 7k, S7i). These data support the view that in inflammatory macrophages, mitochondrial ROS causes DNA damage, which precipitates NAD^+ consumption by PARPs and dependence on NAD^+ salvage.

Complex III is required for inflammatory activation

To explore the role of mitochondrial ROS as a cause of DNA damage, we used specific inhibitors of ETC CI (Rotenone) and CIII (Antimycin A and Myxothiazol (Myx)), which are primary sources of mitochondrial ROS[29]. ROS is produced at two sites in CIII, one on the external face of the inner mitochondrial membrane (CIII Qo), from which ROS can diffuse out of mitochondria, and one on the inner face (CIII Qi), from which ROS is able to diffuse into the mitochondrial matrix[30]. Myx inhibits CIII Qo, whereas Antimycin A inhibits CIII Qi[30]. Pretreatment of macrophages with Myx, but not Rotenone or Antimycin A completely blocked γ-H2AX detected at 1 h post activation (Fig. 8a), but had no effect on cell viability within the experimental timeframe (Supplementary Fig. 8a). Alongside this decrease in DNA damage, Myx treatment also reduced PARP activity (Fig. 8b), production of mitochondrial ROS (Fig. 8c) and upregulation of *Nampt* mRNA in M(γ+LPS) (Fig. 8d). Indicating that ROS from CIII are linked to induced NAD^+ salvage activity in these cells. However, contrary to expectations, Myx treatment did not increase NAD^+ at 1 h (Fig. S8b). Rather it resulted in decreased NAD^+ but increased NADH (Supplementary Fig. 8b), perhaps indicating decreased CI function as an upstream effect of limiting CIII activity.

The dynamic regulation of respiration during the first 4 h following stimulation with γ+LPS or LPS raised the possibility that this change in metabolism is required for cellular activation. Therefore, we asked whether inhibition of CIII between −1 h and +1 h of activation, followed by removal of Myx (which is a reversible inhibitor[31]), and replacement with inhibitor-free medium and γ+LPS, would affect activation status of the cells at 18 h post-stimulation. We found that brief inhibition of CIII during the initial stages of

stimulation with γ+LPS altered the activation profile of the cells, causing an increase in MHCII expression, diminished expression of CD80, NOS2, pro-IL-1β, IL-6 and TNF, and a slight reduction in viability (Fig. 8e-g, Supplementary Fig. 8c). ROS scavenging by NAC had similar effects on inflammatory macrophage polarization, decreasing NOS2 expression, increasing MHC II expression and decreasing IL-6 and TNF production (Supplementary Fig. 8d,e). These effects were more pronounced when NAC was maintained in the culture throughout the 18 h of polarization with γ+LPS (Fig. S8f-h). Considered together, these data suggest that CIII-derived ROS produced during the first hour after stimulation play an important role in inflammatory macrophage activation.

Discussion

Inflammatory macrophage activation is linked to metabolic changes that support and regulate the expression of inflammatory mediators[3, 4, 5, 7]. The most well-studied metabolic transition is a switch to Warburg metabolism, but this is accompanied by alterations in other metabolic processes, including the upregulation of NAD^+ salvage, which is important for sustaining inflammation[10, 11, 12, 13]. Here we explore the underlying basis and functional significance of enhanced NAD^+ salvage in macrophages stimulation with γ+LPS or LPS. Our data indicate that NAD^+ salvage is necessary because of activation-induced mitochondrial ROS production, which leads to ROS-induced DNA damage, and consequently PARP activation with associated NAD^+ consumption. As inflammatory macrophages rely on Warburg metabolism, in which the NAD^+-dependent activity of GAPDH is integral, NAD^+ management assumes critical importance, leaving these cells susceptible to NAMPT inhibition.

We show that NAD^+ pools are rapidly depleted in inflammatory macrophages, compared to resting or alternatively activated macrophages. We attribute early decreases in NAD^+ to the increased activity of PARPs, and reason that ongoing depletion of NAD^+ is due to PARP activity, alongside other factors such as CD38 expression, or the activity of sirtuins, which have been previously shown to utilize NAD^+ at later times during inflammatory macrophage activation[32, 33]. Ongoing NAD^+ depletion is coupled with upregulation of *Nampt* in M(γ+LPS) and M(LPS), and loss of NAMPT activity results in a loss of NAD^+ in these cells, whereas NAD^+ is decreased but not lost in resting macrophages or M(IL-4) under these conditions. These data imply that NAD^+ salvage is a constitutive pathway in macrophages that becomes enhanced and assumes a critical role specifically in inflammatory cells.

Warburg metabolism is a characteristic of cancer cells, and interestingly NAD^+ salvage is upregulated in many cancers[34]. Effects of NAMPT inhibition on tumor growth are suggested to be a consequence of collateral effects on GAPDH function[35]. GAPDH is NAD^+-dependent and when NAD^+ salvage is functioning to maintain NAD^+ pools, inhibition of this pathway would be expected to lead to diminished glycolysis due to loss of GAPDH function. Consistent with this, we found that NAMPT inhibition or knockdown diminished the glycolytic reserve of M(γ+LPS) and M(LPS), but had no effect on this parameter in M0 or M(IL-4). Our data do not exclude the possibility that additional pathways important for activation are also affected by NAMPT inhibition, but do support

the view that Warburg metabolism is induced, is bioenergetically critical, is essential for activation, and is dependent on NAD^+ provided by NAD^+ salvage in M(γ+LPS) and M(LPS).

Consistent with the importance of glycolysis for inflammatory activation[4, 5], and with reported effects of NAMPT inhibition on cytokine production by M(LPS)[10, 11, 12, 13, 33], we found that loss of NAMPT activity resulted in decreased production of many pro-inflammatory mediators by M(γ+LPS) and M(LPS), but also in increased expression of a large set of genes (>2000). Our data indicate that this reflects both transcriptional and post-transcriptional effects, but underlying mechanisms remain to be determined. Interestingly, surface expression of MHC II was increased by NAMPT loss of function, indicating that the ability to present antigen is retained. Together, our data indicate that γ+LPS or LPS activated macrophages in which NAD^+ salvage is limited may be able to assume a distinct function linked to T cell activation, as opposed to inflammation.

As we sought to understand events leading to NAD^+ salvage dependence, we found that rapid depletion of NAD^+ pools coincides with DNA damage. DNA damage in inflammatory macrophages may serve to limit lifespan, facilitate cell-cycle arrest[36] or otherwise affect the fate of these cells[37,38]. Furthermore, the phosphorylation of H2AX (γ-H2AX), could itself play a role in transcriptional regulation[39]. In previous work, DNA damage in macrophages exposed to inflammatory stimuli was attributed largely to NO[23, 24, 37]. However, our findings along with previous work, which aimed to define the phosphoproteome of LPS-activated macrophages[40], revealed significant accumulation of DNA damage very soon after polarization, prior to NO production. This early DNA damage is oxidative, with 8OHG residues present in the nucleus, but also in the cytoplasm. We speculate that cytoplasmic 8OHG signals may represent oxidatively damaged RNA in stress granules, which can form during oxidative stress[41]. The oxidative DNA damage is accompanied by a broad oxidative stress signature, with downregulation of *Keap1* coupled to upregulation of *Nfe2l2* mRNA, Nrf2 protein and transcription of Nrf2-regulated genes. Our data indicate that Nrf2 activation precedes itaconate accumulation (data not shown), which was recently implicated in Nrf2 activation in inflammatory macrophages[42]. We hypothesize that Nrf2 activation occurs directly through ROS destabilization of the KEAP1/Nrf2 complex and, in parallel, altered transcription of the encoding genes.

Our finding that ROS is produced by CIII during the early stages of inflammatory macrophage activation coinciding with transiently increased OXPHOS and SRC, raises the question of why M0 and M(IL-4) macrophages, which exhibit similar or higher rates of respiration and SRC do not accumulate the same oxidative stress. While this could reflect varied efficiency of ROS detoxification, it also may be indicative of a switch in mitochondrial metabolism in inflammatory macrophages, away from ATP production and towards ROS production by the ETC for signaling or anti-microbial purposes, with ATP production compensated for Warburg metabolism[4, 43,44]. Indeed, there is a body of evidence demonstrating important roles for ROS in inflammatory macrophage activation[45, 46, 47, 48]. Here, we show the production of CIII derived ROS in the first hour after stimulation with LPS or γ+LPS is required for production of IL-1β, IL-6 and TNF and expression of CD80 and NOS2.

Collectively, our findings suggest that early ROS production is critical for inflammatory macrophage activation, but also leads to DNA damage and NAD^+ depletion. As a consequence, NAD^+ salvage assumes a critical role. Loss of NAMPT activity results in a reduction in glycolysis due to loss of function of NAD^+-dependent GAPDH, leading to a metabolic crisis and an accompanying failure to produce a subset of inflammatory mediators, which can be rescued by the addition of the NAD^+ salvage metabolite, NMN. Rational targeting of these events may have therapeutic potential in diseases in which inflammatory macrophages are implicated.

Methods

Mice and *in vivo* experiments

C57BL/6 mice (RRID: IMSR_JAX:000664) and B6.129s-Cybb^{tm1Din}/J mice (gp91phox) mice (RRID:ISMR_JAX:002365) were obtained from The Jackson Laboratory, and C57BL/6NRj (C57BL/6N) mice and C57BL/6JRj control mice were obtained from Janvier. All mice were maintained in specific pathogen-free conditions under protocols approved by the animal care committee of the Regierungspräsidium Freiburg, Germany, in compliance with all relevant ethical regulations. All animals used for tissue harvest or experimental procedures were aged between 6–9 weeks of age. Animals were humanely sacrificed by carbon dioxide asphyxiation followed by cervical dislocation, and bone marrow, peritoneal lavage, and epididymal adipose tissue were harvested post mortem.

For *in vivo* studies, mice were injected intraperitoneally (i.p.) with 8 mg/kg LPS (Sigma, further details for all reagents are supplied in the “Life Sciences Reporting Summary”), and body temperature was monitored for the duration of the experiment using an infrared thermometer (Bioseb). Mice were administered FK866 (10 mg/kg, i.p.; Tocris) or an equivalent volume of solvent (DMSO, control) 12 h prior to, and at the time of, LPS delivery. Blood was collected by lateral tail vein bleeding 1.5 h (for TNF analysis) or 3 h (for IL-1β and IL-6 analysis), after LPS delivery, and serum cytokines were analyzed by ELISA. Mice were sacrificed 12 h after LPS administration.

Primary cell cultures

Bone marrow cells were grown in complete media (RPMI-1640 medium containing 10 mM glucose, 2 mM L-Glutamine, 100 U/ml penicillin-streptomycin and 10% FCS) with 20 ng/ml murine macrophage colony stimulating factor 1 (CSF-1; Peprotech) for 7 days, and supplemented with CSF-1 on days 3 and 5. On day 7 macrophages were harvested and all cells continued to be maintained in 20 ng/ml CSF-1; M(γ+LPS) were stimulated with 50 ng/ml IFN-γ (R & D systems) and 20 ng/ml LPS (Sigma); M(LPS) were stimulated with 100 ng/ml LPS; M(IL-4) were stimulated with 20 ng/ml IL-4 (Peprotech) for the indicated times. Treatment with inhibitors was performed for the duration of stimulation, unless otherwise stated. Cells were treated with 50 nM FK866 (Tocris) unless otherwise indicated in the figure legend, 50 nM GPP78 (Tocris), 50 nM STF118804 (Tocris),1 μM Heptelidic acid (Cayman Chemicals), 1 mM NMN (Sigma), 2 μM - 10 μM Rucaparib (Sigma), 10 mM N-acetyl-cysteine (NAC; Sigma), 100 μM MitoTempol (Abcam), 100 μM

Tempol (Santa Cruz), 200 nM Myxothiazol (Sigma), 1 μM Antimycin A (Sigma), 100 nM Rotenone (Sigma) or 1 μM Oligomycin (Sigma).

After naive or LPS-challenged mice were sacrificed, peritoneal macrophages were harvested by peritoneal lavage with sterile PBS containing 2 mM EDTA (Thermo Fisher Scientific) at a volume of 5 ml per mouse. Cells were counted, and plated in complete RPMI supplemented with CSF-1 and selected based on adherence. Epididymal fat was also harvested from these mice, and digested in DMEM low 1 g/L glucose (Thermo Fisher Scientific), supplemented with 1% bovine serum albumin (Sigma), 50 mM HEPES pH 7.2–7.5 (Gibco) and 2 mg/ml Collagenase II (Gibco) for 30 min at 37°C. Stromal cells were counted, plated in complete RPMI supplemented with CSF-1 and selected based on adherence. All cell culture was performed under 5% CO_2, atmospheric oxygen, at 37°C in a humidified incubator.

Lentiviral and retroviral production and cell transduction

HEK293T cells were transfected using Lipofectamine 3000 (Thermo Fisher Scientific) with lentiviral packaging vectors pCAG-eco and psPAX.2 plus empty pLKO.1 control with a Puromycin selection cassette (all Adgene) or a shRNA containing pLKO.1 targeting *NAMPT* (GE Dharmacon Cat# RMM4534-EG59027 – TRCN0000101279). Virus was collected in the supernatant of the cells. Bone marrow cultures were transduced by centrifugation for 90 min (1300 x *g*) in the presence of polybrene (8 mg/ml) on day 2 of culture. 48 h selection of transduced cells was performed with 6 μg/ml puromycin (Sigma).

RNA-seq

Total RNA was extracted with the RNAqueous-Micro Total RNA Isolation Kit (Thermo Fisher Scientific) and quantified using Qubit 2.0 (Thermo Fisher Scientific) following the manufacturer's instructions. Libraries were prepared using the TruSeq stranded mRNA kit (Illumina) and sequenced in a HISeq 3000 (Illumina) by the Deep-sequencing Facility at the Max-Planck-Institute for Immunobiology and Epigenetics. Sequenced libraries were processed with the Galaxy platform and deepTools[49, 50] using STAR[51], for trimming and mapping, and featureCounts[52] to quantify mapped reads. Raw mapped reads were processed in R (Lucent Technologies) with DESeq2[53], to determine differentially expressed genes and generate normalized read counts to visualize as heatmaps using Morpheus (Broad Institute).

Flow cytometry and confocal microscopy

Cells were kept at 4°C, blocked with 5 μg/ml anti-CD16/32 (Biozol), stained with Live Dead Fixable Aqua or Live Dead Fixable Blue (Life Technologies), then surface stained with fluorochrome-conjugated monoclonal antibodies to: CD45 (BioLegend, clone: 30-F11), CD11b (BioLegend, clone: M1/70), CD11c (BioLegend, clone: N418), CD80 (Thermo Fisher Scientific, clone: 16–10A1), CD86 (BioLegend, clone: Gl-1), CD206 (BioLegend, clone: CO68C2), CD301 (Miltenyi Biotech, clone: REA687), F4/80 (eBioscience or Biozol, clone: BM8), Ly6C (BioLegend, clone: HK1.4), Ly6G (BioLegend, clone:1A8), MHC II (eBioscience, clone: M5/114.15.2), Siglec F (BioLegend, clone: E50–2440), Tim4 (BioLegend, clone: F31–5G3). For intracellular staining, cells were fixed and permeabilized (BD FoxP3 FixPerm Kit) and stained with fluorochrome-conjugated antibodies to

phosphorylated H2AX (γ-H2AX; BD Biosciences, clone: N1–431), NOS2 (Santa Cruz, clone: C-11), and TNF (eBioscience, clone: TN3–19.12). RELMα primary antibody staining (Peprotech Cat# 500-P214) was detected using pacific blue anti-rabbit secondary antibody (Life Technologies). For mitochondrial superoxide staining adherent cells in culture were incubated with 5 μM MitoSOX (Thermo Fisher Scientific) in HBSS/Ca/Mg (Sigma) for 10 min, then washed, harvested and resuspended in FACS buffer containing DAPI (Cell Signaling Technologies). Data was acquired by flow cytometry on an LSRII or LSR Fortessa (BD Biosciences) and analyzed with FlowJo v.10.1 (Tree Star).

For confocal microscopy 2×10^5 BMDM were plated on a 10 mm poly-D-lysine coated cover slide, in a 24 well plate. BMDMs were subsequently stimulated with LPS, γ+LPS, IL-4 or CSF-1 alone for 1 h. Cells were then fixed with 100 μL CytoFix/CytoPerm (Biolegend) for 40 min followed by blocking with PBS/BSA 1% for 30 min. BMDM were stained for 8OHg (Abcam 62623, 1:50) on ice to reduce non-specific binding for 40 min. The cells were washed with wash buffer (BioLegend) and stained with fluorescence secondary antibody (Invitrogen, 1:250) for 30 min. Slides were mounted with Vectashield with DAPI and sealed with nail polish prior to image acquisition using a Zeiss LSM 880 with Aryscan equipped with a 63× objective. Confocal images were analyzed and merged using ImageJ software. The antibody was validated with a species-specific IgG-negative control at the same concentration.

Metabolic assays

Real-time ECAR and OCR measurements were made with an XF-96 Extracellular Flux Analyzer (Seahorse Bioscience). 1×10^5 BMDMs, or 2×10^5 pMacs or adipose tissue macrophages were plated into each well of seahorse X96 cell culture microplates, and preincubated at 37°C for a minimum of 45 min in the absence of CO_2 in un-buffered RPMI with 1 mM pyruvate, 2 mM L-glutamine and 25 mM glucose for mitochondrial stress test or without glucose for glycolytic stress test, with pH adjusted to 7.4. OCR and ECAR were measured under basal conditions and after the addition of the following compounds: 10 mM glucose, 1 μM oligomycin, 1.5 μM flurocarbonyl cyanide phenylhydrazon (FCCP), 100 nM rotenone + 1 μM antimycin, and 50 mM 2DG (all Sigma) as indicated. Results were collected with Wave software version 2.4 (Agilent).

Glucose and lactate were measured in cell culture supernatants with the Cedex Bioanalyser (Roche).

Metabolite quantitation of stimulated macrophages was performed with mass spectrometry by liquid chromatography coupled to tandem mass spectrometry (LCMS) by the Metabolomics Core, Max-Planck-Institute for Immunobiology and Epigenetics, Freiburg, Germany and University of California – Los Angeles Metabolomics Centre, Los Angeles, USA. For general metabolite quantification cells were washed and metabolites were extracted twice with methanol (80%). For NAD^+ quantification by LCMS cells were washed with PBS and metabolites were extracted three times by acidic acetonitrile extraction (adapted from Lu et al 2018[54]). Detection of other redox intermediates, specifically NADH and NADPH was challenging in macrophages and required an increased number of cells than was the case for the other metabolites measured here.

NAD^+ abundance was also measured using the NAD^+/NADH quantitation colorimetric kit (Biovision), as per manufacturer's instructions with the sole modification of 2×10^5 cells extracted in 200 μL extraction buffer.

Mitochondrial ROS were measured as described above.

ATP abundance was measured using the ATP determination kit (Thermo Fisher Scientific). Cells were resuspended in water at 1000 cells/μL, boiled for 10 min at 95°C then lysates were analyzed as per the manufacturer's instructions.

Nitrites in cell culture supernatants were measured by Greiss reaction (Greiss reagent kit for Nitrite Determination; Thermo Fisher) according to manufacturer's instructions.

ELISAs

Cell culture supernatants, peritoneal lavage or serum were collected and IL-1β, IL-6, and TNF concentrations were assayed by ELISA (BioLegend ELISA Max kits), as per manufacturer's instructions. Absorbance was measured using a TriStar plate reader (Berthold Technologies). Standard curves were analyzed in Prism using 'second-order polynomial interpolation'.

PARP activity was determined in cell lysates using the HT PARP *In Vivo* Pharmacodynamic Assay II Kit (Trevigen), as per manufacturers instructions, with two modifications – 1×10^6 cells were utilized per sample, and samples were diluted 1:10 to be within the range of the standard curve. Chemiluminescence was measured using a TriStar plate reader (Berthold Technologies). Standard curves were analyzed in Prism using 'linear interpolation'.

Immunoblotting

Cells were washed with cold PBS, centrifuged at 400 × *g* for 5 min at 4°C, then lysed. For pro-IL-1β, cells were lysed in 1 × Cell Signaling lysis buffer (20 mM Tris-HCl, [pH 7.5], 150 mM NaCl, 1 mM Na_2EDTA, 1 mM EGTA, 1% Triton X-100, 2.5 mM sodium pyrophosphate, 1 mM beta-glycerophosphate, 1 mM Na_3VO_4, 1 mg/ml leupeptin; Cell Signaling Technologies) supplemented with 1 mM PMSF (Sigma). Samples were frozen and thawed 3 times to lyse. For γ-H2AX immunoblots cells were lysed in RIPA buffer (Sigma) and supplemented with 1 mM PMSF and 1x Cell Signaling protease/phosphatase inhibitor cocktail. Samples were chilled on ice for 50 min, vortexing every 10 min, and subsequently were sonicated for 15s with 45s rests; sonication was repeated 5 times. Lysates were centrifuged at 20,000 × *g* for 10 min at 4°C. Cleared lysates were denatured with LDS loading buffer supplemented with 50 mM dithiothreitol (Sigma) for 10 min at 70°C and loaded on precast 4% to 12% bis-tris protein gels (Thermo Fisher Scientific). Proteins were transferred onto nitrocellulose membranes using the iBLOT 2 system (Thermo Fisher Scientific) following the manufacturer's protocols. Membranes were blocked with 5% milk in TBS with 0.1% Tween-20 and incubated with the appropriate antibodies in 5% (w/v) BSA in TBS with 0.1% Tween-20 overnight at 4°C. Antibodies against pro-IL-1β (Cell Signaling Technologies), tubulin (Abcam), actin (Cell Signaling Technologies), NAMPT (Adipogen), Nrf2 (Cell Signaling Technologies) and phospho-H2AX (Millipore) were used. Primary antibody incubations were followed by incubation with secondary HRP-conjugated antibody

(Pierce) in 5% milk in TBS with 0.1% Tween-20 and visualized using SuperSignal West Pico or femto Chemiluminescent Substrate (Pierce) on Hyperfilm Mp (Millipore).

Gene expression analysis by qRT-PCR

RNA was extracted from lysates with the RNeasy kit (Qiagen), quantified using a Qubit, and cDNA was synthesized with the high-capacity RNA to cDNA kit (Applied Biosystems) following the manufacturers' instructions. qPCR was performed on the QuantStudio3 (Thermo Fisher Scientific) using the DreamTaq Green PCR Master Mix (2x; Biorad), and the following probe sets: *Nampt* (Mm00451938_m1), *Hprt* (Mm03024075_m1) (all Applied Biosystems). Results were analyzed by the 2−ΔΔCt method using *Hprt* as a housekeeping gene.

Statistical Analysis

Statistical analysis was performed using prism 6 software (Graph pad) and results are represented as mean ± SEM, unless otherwise indicated. Comparisons for two groups were calculated using unpaired two-tailed Student's *t* tests, comparisons of more than two groups were calculated using one-way ANOVA with Tukey's correction for multiple comparisons. We observed normal distribution and no difference in variance between groups in individual comparisons. Selection of sample size was based on extensive experience with metabolic assays.

Supplementary Material

Refer to Web version on PubMed Central for supplementary material.

Acknowledgements

We would like to thank members of the Pearce laboratories for support and discussion and B. Sleckman and A. Morales at Cornell Weill for their generous advice during these studies. We also thank D. Braas and the UCLA Metabolomics Centre and the DeepSequencing facility at the MPI-IE for their technical support. This work was funded by NIH grants AI 110481 (E.J.P.) and CA18125 (E.L.P.), a Sir Henry Wellcome Fellowship awarded by The Wellcome Trust (D.J.P.), and the Max Planck Society (E.J.P and E.L.P).

Data Availability

All data generated or analyzed during this study are included in this published article (and its supplementary information) and the data that support the findings of this study are available from the corresponding author upon reasonable request. Next generation sequencing data can be accessed at Gene Expression Omnibus under the accession number GSE123596.

References

1. Wynn TA, Chawla A. & Pollard JW Macrophage biology in development, homeostasis and disease. Nature 496, 445–455 (2013). [PubMed: 23619691]
2. Huang SC et al. Cell-intrinsic lysosomal lipolysis is essential for alternative activation of macrophages. Nat Immunol 15, 846–855 (2014). [PubMed: 25086775]
3. Jha AK et al. Network integration of parallel metabolic and transcriptional data reveals metabolic modules that regulate macrophage polarization. Immunity 42, 419–430 (2015). [PubMed: 25786174]

4. Mills EL et al. Succinate Dehydrogenase Supports Metabolic Repurposing of Mitochondria to Drive Inflammatory Macrophages. Cell 167, 457–470 e413 (2016). [PubMed: 27667687]
5. Tannahill GM et al. Succinate is an inflammatory signal that induces IL-1beta through HIF-1alpha. Nature 496, 238–242 (2013). [PubMed: 23535595]
6. Krawczyk CM et al. Toll-like receptor-induced changes in glycolytic metabolism regulate dendritic cell activation. Blood 115, 4742–4749 (2010). [PubMed: 20351312]
7. O'Neill LA & Pearce EJ Immunometabolism governs dendritic cell and macrophage function. J Exp Med 213, 15–23 (2016). [PubMed: 26694970]
8. Locasale JW & Cantley LC Metabolic flux and the regulation of mammalian cell growth. Cell Metab 14, 443–451 (2011). [PubMed: 21982705]
9. Verdin E. NAD(+) in aging, metabolism, and neurodegeneration. Science 350, 1208–1213 (2015). [PubMed: 26785480]
10. Busso N. et al. Pharmacological inhibition of nicotinamide phosphoribosyltransferase/visfatin enzymatic activity identifies a new inflammatory pathway linked to NAD. PLoS One 3, e2267 (2008). [PubMed: 18493620]
11. Halvorsen B. et al. Increased expression of NAMPT in PBMC from patients with acute coronary syndrome and in inflammatory M1 macrophages. Atherosclerosis 243, 204–210 (2015). [PubMed: 26402139]
12. Liu TF, Yoza BK, El Gazzar M, Vachharajani VT & McCall CE NAD+-dependent SIRT1 deacetylase participates in epigenetic reprogramming during endotoxin tolerance. J Biol Chem 286, 9856–9864 (2011). [PubMed: 21245135]
13. Schilling E. et al. Inhibition of nicotinamide phosphoribosyltransferase modifies LPS-induced inflammatory responses of human monocytes. Innate Immun 18, 518–530 (2012). [PubMed: 21975728]
14. Galli M, Van Gool F, Rongvaux A, Andris F. & Leo O. The nicotinamide phosphoribosyltransferase: a molecular link between metabolism, inflammation, and cancer. Cancer Res 70, 8–11 (2010). [PubMed: 20028851]
15. Gerner RR et al. NAD metabolism fuels human and mouse intestinal inflammation. Gut 67, 1813–1823 (2018). [PubMed: 28877980]
16. Hasmann M. & Schemainda I. FK866, a highly specific noncompetitive inhibitor of nicotinamide phosphoribosyltransferase, represents a novel mechanism for induction of tumor cell apoptosis. Cancer Res 63, 7436–7442 (2003). [PubMed: 14612543]
17. Ronchi JA et al. A spontaneous mutation in the nicotinamide nucleotide transhydrogenase gene of C57BL/6J mice results in mitochondrial redox abnormalities. Free Radical Biology and Medicine 63, 446–456 (2013). [PubMed: 23747984]
18. Everts B. et al. Commitment to glycolysis sustains survival of NO-producing inflammatory dendritic cells. Blood 120, 1422–1431 (2012). [PubMed: 22786879]
19. Tan B. et al. Inhibition of Nicotinamide Phosphoribosyltransferase (NAMPT), an Enzyme Essential for NAD+ Biosynthesis, Leads to Altered Carbohydrate Metabolism in Cancer Cells. The Journal of biological chemistry 290, 15812–15824 (2015). [PubMed: 25944913]
20. Liberti MV et al. A Predictive Model for Selective Targeting of the Warburg Effect through GAPDH Inhibition with a Natural Product. Cell Metab 26, 648–659 e648 (2017). [PubMed: 28918937]
21. Barth MW, Hendrzak JA, Melnicoff MJ & Morahan PS Review of the macrophage disappearance reaction. Journal of Leukocyte Biology 57, 361–367 (1995). [PubMed: 7884305]
22. Dockery LE, Gunderson CC & Moore KN Rucaparib: the past, present, and future of a newly approved PARP inhibitor for ovarian cancer. Onco Targets Ther 10, 3029–3037 (2017). [PubMed: 28790837]
23. Morales AJ et al. A type I IFN-dependent DNA damage response regulates the genetic program and inflammasome activation in macrophages. Elife 6, e24655 (2017).
24. Zingarelli B, O'Connor M, Wong H, Salzman AL & Szabo C. Peroxynitrite-mediated DNA strand breakage activates poly-adenosine diphosphate ribosyl synthetase and causes cellular energy depletion in macrophages stimulated with bacterial lipopolysaccharide. J Immunol 156, 350–358 (1996). [PubMed: 8598485]

25. Hayes JD & Dinkova-Kostova AT The Nrf2 regulatory network provides an interface between redox and intermediary metabolism. Trends Biochem Sci 39, 199–218 (2014). [PubMed: 24647116]
26. Nunes P, Demaurex N. & Dinauer MC Regulation of the NADPH oxidase and associated ion fluxes during phagocytosis. Traffic 14, 1118–1131 (2013). [PubMed: 23980663]
27. Samuni Y, Goldstein S, Dean OM & Berk M. The chemistry and biological activities of N-acetylcysteine. Biochim Biophys Acta 1830, 4117–4129 (2013). [PubMed: 23618697]
28. Ezeriņa D, Takano Y, Hanaoka K, Urano Y. & Dick TP N-Acetyl Cysteine Functions as a Fast-Acting Antioxidant by Triggering Intracellular H2S and Sulfane Sulfur Production. Cell Chemical Biology 25, 447–459.e444 (2018). [PubMed: 29429900]
29. Murphy MP How mitochondria produce reactive oxygen species. Biochem J 417, 1–13 (2009). [PubMed: 19061483]
30. Bleier L. & Drose S. Superoxide generation by complex III: from mechanistic rationales to functional consequences. Biochim Biophys Acta 1827, 1320–1331 (2013). [PubMed: 23269318]
31. Conradt P, Dittmar KE, Schliephacke H. & Trowitzsch-Kienast W. Myxothiazol: a reversible blocker of the cell cycle. J Antibiot (Tokyo) 42, 1158–1162 (1989). [PubMed: 2753821]
32. Matalonga J. et al. The Nuclear Receptor LXR Limits Bacterial Infection of Host Macrophages through a Mechanism that Impacts Cellular NAD Metabolism. Cell Rep 18, 1241–1255 (2017). [PubMed: 28147278]
33. Van Gool F. et al. Intracellular NAD levels regulate tumor necrosis factor protein synthesis in a sirtuin-dependent manner. Nat Med 15, 206–210 (2009). [PubMed: 19151729]
34. Sampath D, Zabka TS, Misner DL, O'Brien T. & Dragovich PS Inhibition of nicotinamide phosphoribosyltransferase (NAMPT) as a therapeutic strategy in cancer. Pharmacol Ther 151, 16–31 (2015). [PubMed: 25709099]
35. Tan B. et al. Pharmacological inhibition of nicotinamide phosphoribosyltransferase (NAMPT), an enzyme essential for NAD+ biosynthesis, in human cancer cells: metabolic basis and potential clinical implications. J Biol Chem 288, 3500–3511 (2013). [PubMed: 23239881]
36. Jackson SP & Bartek J. The DNA-damage response in human biology and disease. Nature 461, 1071–1078 (2009). [PubMed: 19847258]
37. Pereira-Lopes S. et al. NBS1 is required for macrophage homeostasis and functional activity in mice. Blood 126, 2502–2510 (2015). [PubMed: 26324700]
38. Herrtwich L. et al. DNA Damage Signaling Instructs Polyploid Macrophage Fate in Granulomas. Cell 167, 1264–1280 e1218 (2016). [PubMed: 28084216]
39. Singh I. et al. High mobility group protein-mediated transcription requires DNA damage marker gamma-H2AX. Cell Res 25, 837–850 (2015). [PubMed: 26045162]
40. Weintz G. et al. The phosphoproteome of toll-like receptor-activated macrophages. Mol Syst Biol 6, 371 (2010). [PubMed: 20531401]
41. Leung A, Todorova T, Ando Y. & Chang P. Poly(ADP-ribose) regulates post-transcriptional gene regulation in the cytoplasm. RNA Biol 9, 542–548 (2012). [PubMed: 22531498]
42. Mills EL et al. Itaconate is an anti-inflammatory metabolite that activates Nrf2 via alkylation of KEAP1. Nature 556, 113–117 (2018). [PubMed: 29590092]
43. Palsson-McDermott EM & O'Neill LA The Warburg effect then and now: from cancer to inflammatory diseases. Bioessays 35, 965–973 (2013). [PubMed: 24115022]
44. Garaude J. et al. Mitochondrial respiratory-chain adaptations in macrophages contribute to antibacterial host defense. Nat Immunol 17, 1037–1045 (2016). [PubMed: 27348412]
45. Nakahira K. et al. Autophagy proteins regulate innate immune responses by inhibiting the release of mitochondrial DNA mediated by the NALP3 inflammasome. Nat Immunol 12, 222–230 (2011). [PubMed: 21151103]
46. West AP et al. TLR signalling augments macrophage bactericidal activity through mitochondrial ROS. Nature 472, 476–480 (2011). [PubMed: 21525932]
47. Park J. et al. Mitochondrial ROS govern the LPS-induced pro-inflammatory response in microglia cells by regulating MAPK and NF-kappaB pathways. Neurosci Lett 584, 191–196 (2015). [PubMed: 25459294]

48. Bulua AC et al. Mitochondrial reactive oxygen species promote production of proinflammatory cytokines and are elevated in TNFR1-associated periodic syndrome (TRAPS). J Exp Med 208, 519–533 (2011). [PubMed: 21282379]

49. Afgan E. et al. The Galaxy platform for accessible, reproducible and collaborative biomedical analyses: 2016 update. Nucleic Acids Res 44, W3–W10 (2016). [PubMed: 27137889]

50. Ramirez F. et al. deepTools2: a next generation web server for deep-sequencing data analysis. Nucleic Acids Res 44, W160–165 (2016). [PubMed: 27079975]

51. Dobin A. et al. STAR: ultrafast universal RNA-seq aligner. Bioinformatics 29, 15–21 (2013). [PubMed: 23104886]

52. Liao Y, Smyth GK & Shi W. featureCounts: an efficient general purpose program for assigning sequence reads to genomic features. Bioinformatics 30, 923–930 (2014). [PubMed: 24227677]

53. Love MI, Huber W. & Anders S. Moderated estimation of fold change and dispersion for RNA-seq data with DESeq2. Genome Biol 15, 550 (2014). [PubMed: 25516281]

54. Lu W, Wang L, Chen L, Hui S. & Rabinowitz JD Extraction and Quantitation of Nicotinamide Adenine Dinucleotide Redox Cofactors. Antioxid Redox Signal 28, 167–179 (2018). [PubMed: 28497978]

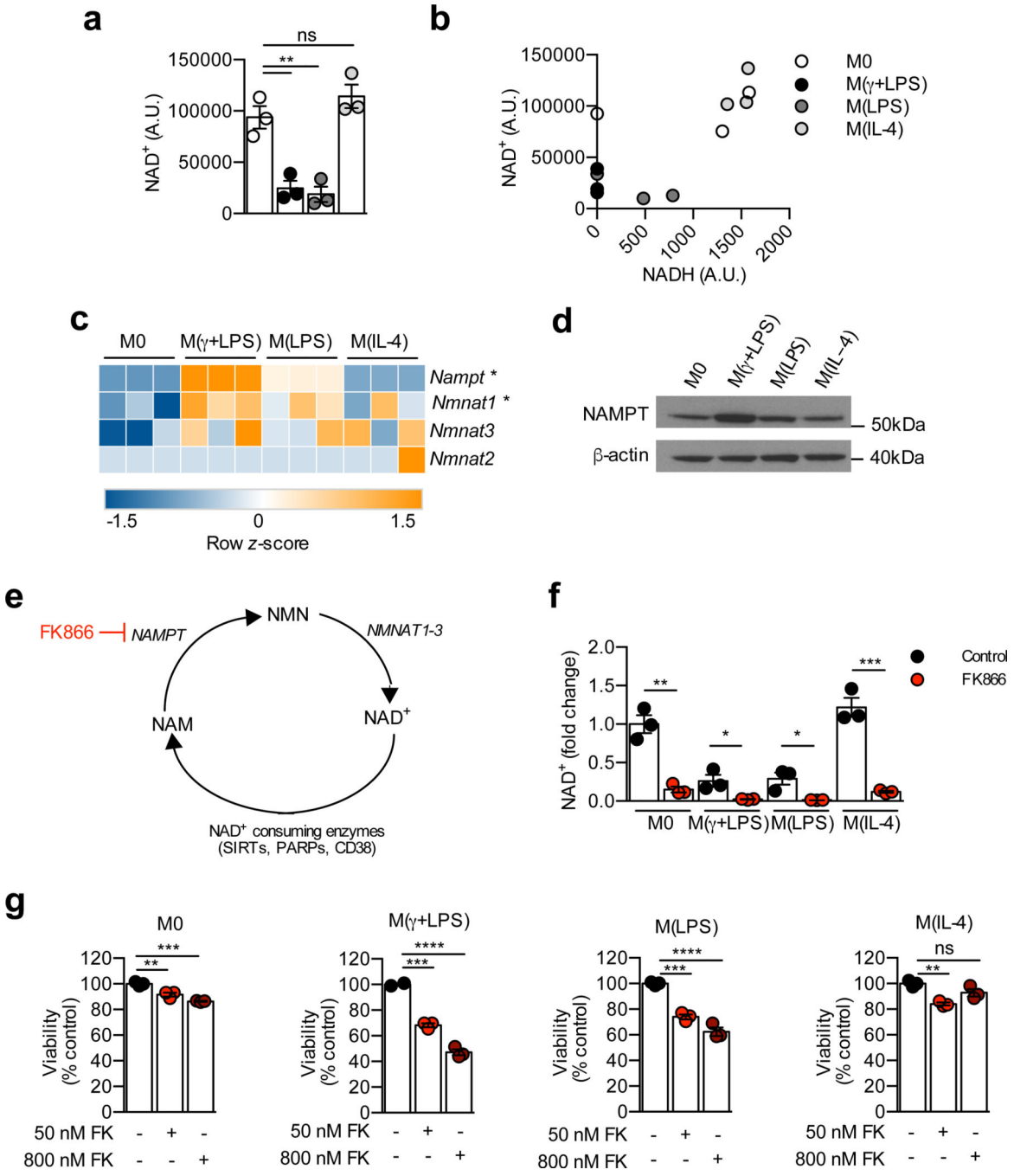

Figure 1: NAD$^+$ is depleted in inflammatory macrophages, and NAD$^+$ salvage is required for viability.

(**a**) NAD$^+$ and (**b**) NAD$^+$ and NADH in M0, M(γ+LPS), M(LPS) and M(IL-4) polarized for 18 h, quantified by LC-MS based on area under the curve, A.U. represent arbitrary units (n= 3 biologically independent samples, representative of four independent experiments). (**c**) RNA-seq analysis of NAD$^+$ salvage gene expression in M0, M(γ+LPS), M(LPS) and M(IL-4) polarized for 18 h. Statistically significant (adjusted p value < 0.1) upregulated (> 2 fold) genes denoted by * in M(γ+LPS) compared to M0 (n= 3 biologically independent

samples). (**d**) NAMPT and β-actin (loading control) expression by immunoblotting in M0, M(γ+LPS), M(LPS) and M(IL-4) polarized for 18 h. The blot was cropped to show relevant bands and is representative of three independent experiments with similar results. (**e**) Schematic representation of the NAD^+ salvage pathway. NAD^+ levels (**f**) and survival (**g**) of M0, M(γ+LPS), M(LPS) and M(IL-4) cultured for 18 h in the presence or absence of FK866 (**f,** 50 nM, and **g,** 50 nM or 800 nM). NAD^+ shown relative to M0, and viability relative to appropriate control macrophages (n= 3 biologically independent samples, representative of three independent experiments). Data were analyzed in **a,g** by one-way analysis of variance (ANOVA) with Tukey's multiple comparison test, in **f** by unpaired, two-sided Student's *t*-test. Error bars are mean ± SEM. *p < 0.05, **p < 0.01, ***p < 0.001 and ****p < 000.1.

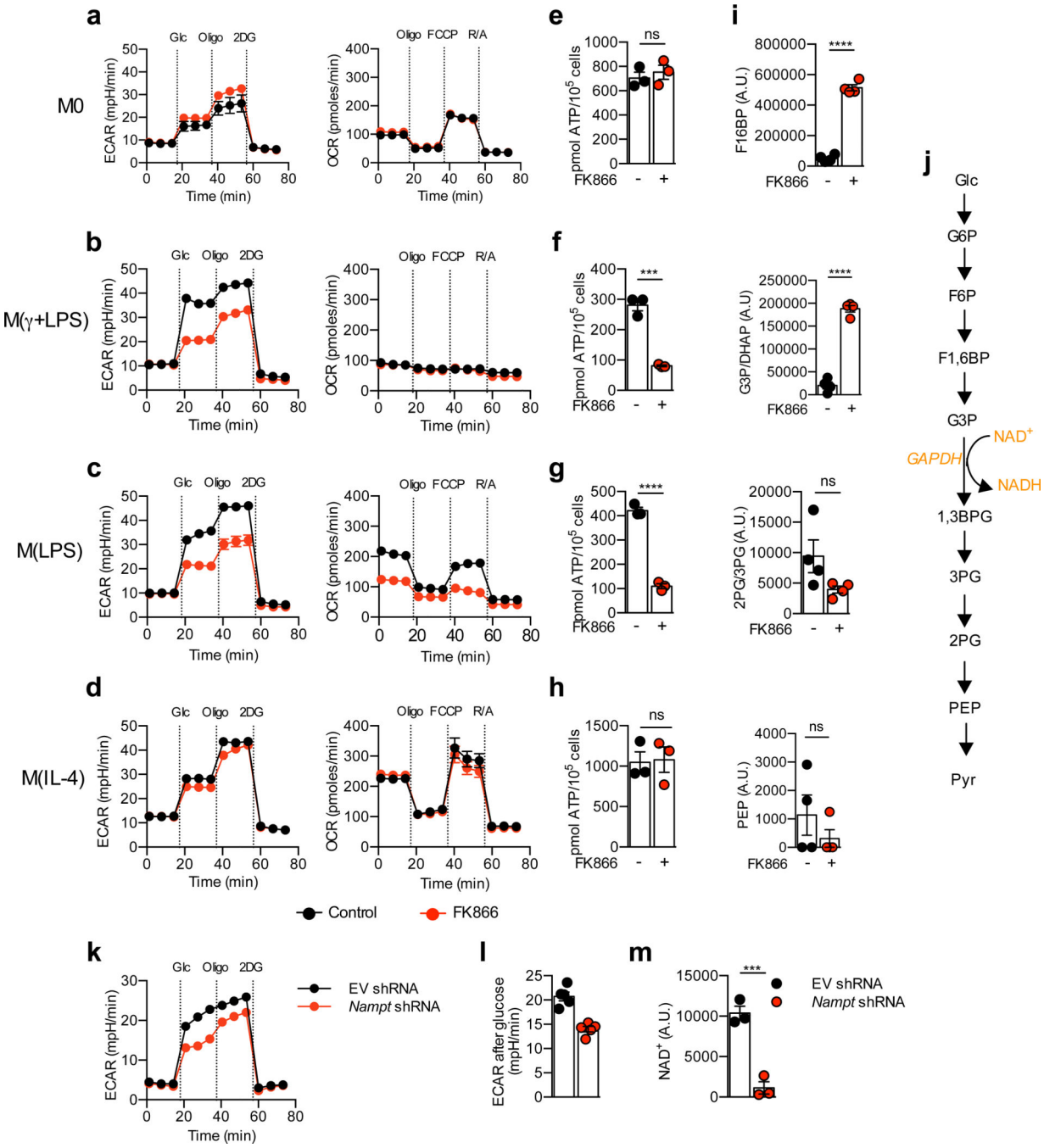

Figure 2: NAD$^+$ salvage regulates the core metabolism of inflammatory macrophages through changes in GAPDH activity.

Real-time changes in the ECAR and OCR of M0 (**a**), M(γ+LPS) (**b**), M(LPS) (**c**) and M(IL-4) (**d**), untreated or treated with 50 nM FK866 for 18 h measured using Seahorse (*n* = five technical replicates in **a,b,d** and four technical replicates in **c.** Data in **a,d** are representative of four independent experiments, and in **c,d** are representative of more than ten independent experiments). ATP quantification of M0 (**e**), M(γ+LPS) (**f**), M(LPS) (**g**) and M(IL-4) (**h**) untreated or treated with 50 nM FK86. (*n* = 3 biologically

independent samples, representative of three independent experiments.) (**i**) LC-MS analysis of glycolytic metabolites in control M(γ+LPS) or M(γ+LPS) treated with 50 nM FK866 (*n* = 4 biologically independent samples, representative of five independent experiments). (**j**) Schematic representation of glycolysis. Real-time changes in the ECAR (**k**) and ECAR after glucose injection (**l**) of M(γ+LPS) transduced with empty vector or *Nampt* shRNA and polarized for 18h, measured using Seahorse. (*n* = five technical replicates, representative of five independent experiments). (**m**) NAD^+ levels of M(γ+LPS) transduced with empty vector or *Nampt* shRNA and polarized for 18h, as analysed by LC-MS (*n* = 3 biologically independent samples, representative of two independent experiments.). Data were analyzed by unpaired, two-sided Student's *t*-test. Error bars are mean ± SEM. *p < 0.05, **p < 0.01, ***p < 0.001 and ****p < 000.1.

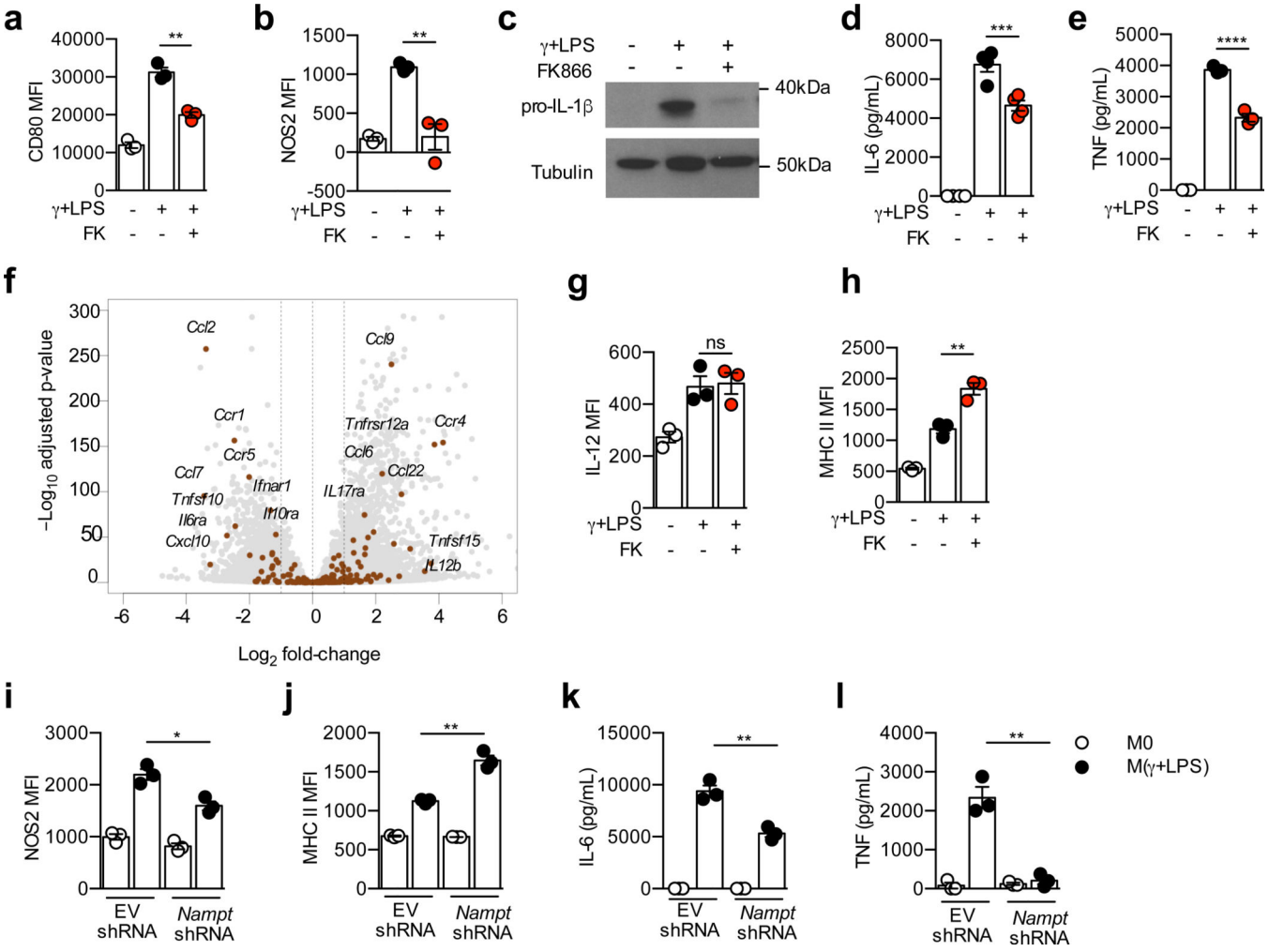

Figure 3: NAMPT loss of function modulates inflammatory macrophage activation.

(**a-e**) M(γ+LPS) were polarized for 18h with or without FK866 treatment. CD80 (**a**) and NOS2 (**b**) expression were analyzed by flow cytometry (*n* = 3 biologically independent samples, representative of over ten independent experiments). (**c**) pro-IL-1β was assessed by immunoblot. The blot was cropped to show relevant bands, and is representative of three independent experiments with similar results. IL-6 (**d**) and TNF (**e**) production were assessed by ELISA (**d,** *n* = 4 biologically independent samples, **e**, *n* = 3 biologically independent samples. Both representative of five independent experiments.). (**f**) Volcano plot of differentially expressed genes in untreated M(γ+LPS) compared to FK966 treated M(γ+LPS) after 18 h of culture, highlighting expression of cytokine related genes obtained from the Kyoto Encyclopedia of genes and genomes (*n* = 3 biologically independent samples). IL-12p40 (**g**) and MHC II (**h**) expression in M(γ+LPS) polarized with or without FK866 for 18 h, as measured by flow cytometry (*n* = 3 biologically independent samples, representative of three (**g**) and over ten (**h**) independent experiments). Expression of NOS2 (**i**) and MHC II (**j**) and cytokines IL-6 (**k**) and TNF (**l**) in M0 and M(γ+LPS) transduced with empty vector or *Nampt* shRNA and polarized for 18h, analyzed by flow cytometry (**i,j**), or ELISA (k,**l**) (*n* = 3 biologically independent samples, representative of three independent

experiments). Error bars are mean ± SEM and were analyzed by unpaired, two-sided Student's *t*-test. *p < 0.05, **p < 0.01, ***p < 0.001 and ****p < 000.1

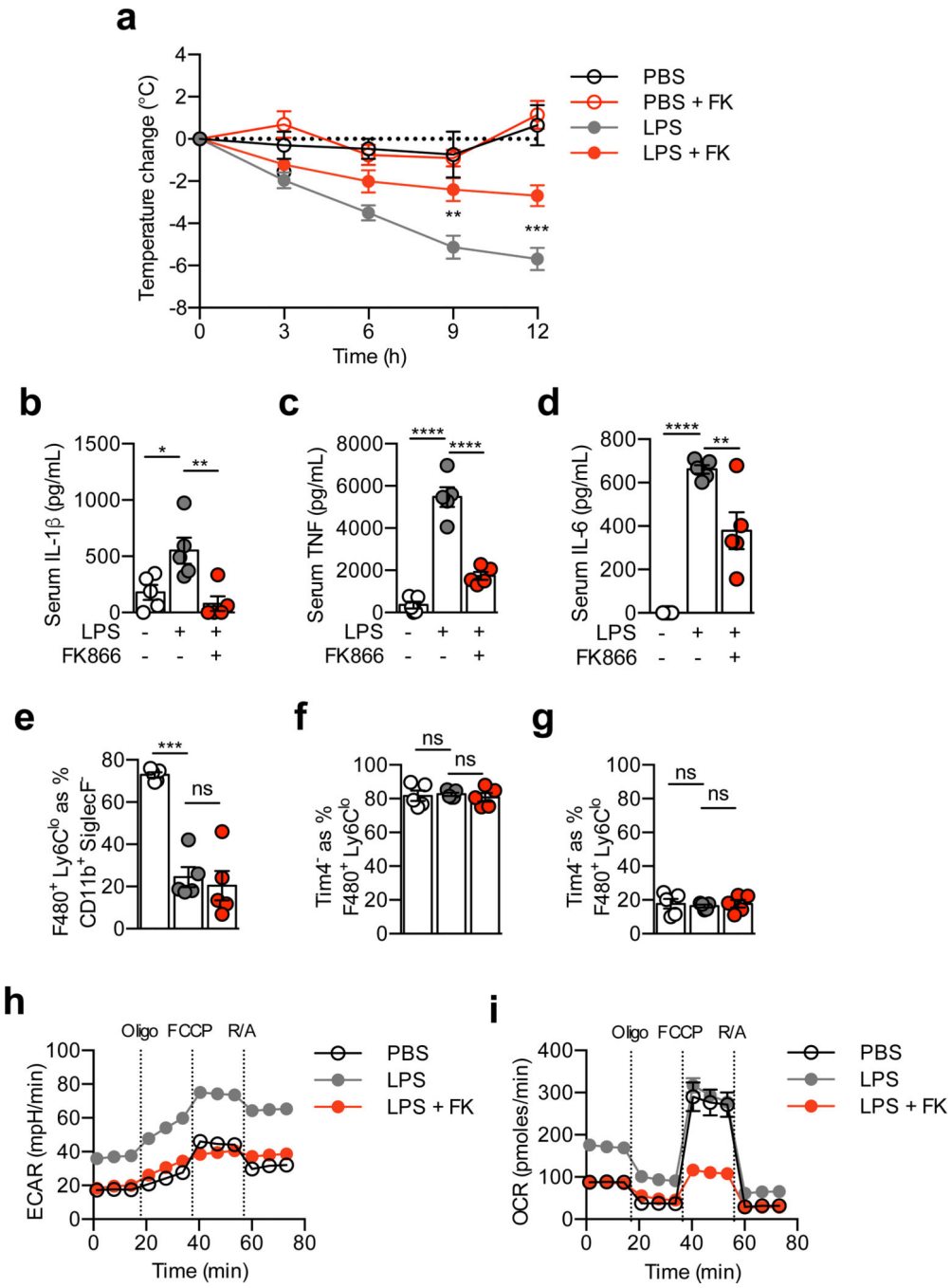

Figure 4: NAMPT inhibition reduces *in vivo* inflammation, modulating inflammatory macrophage metabolism

(**a**) Mice were given i.p. PBS, FK866, LPS or LPS and FK866 and body temperature was measured by infrared sensor, change in body temperature displayed relative to 0 h time-point (n = 5 mice, representative of five independent experiments). Blood samples were collected at 1.5 or 3 hours after delivery of LPS and serum IL-1β (**b**), TNF (**c**), and IL-6 (**d**) were assessed (n = 5 mice, representative of two (**b**) or three (**c,d**) independent experiments). Peritoneal lavage was collected 12 h after LPS administration and total macrophage (**e**), and

Tim4^{+} resident macrophages (**f**) and Tim4^{-} macrophages (**g**) frequency was assessed (n = 5 mice, representative of two independent experiments). Real time changes in the ECAR (**h**) and OCR (**i**) of peritoneal macrophages isolated from mice given i.p. PBS, LPS or LPS and FK866 (n = six technical replicates from five pooled biological samples, representative of three independent experiments). Error bars are mean ± SEM. Data were analyzed in **a** by two-way ANOVA with Tukey's multiple comparison test, and by one-way ANOVA with Tukey's multiple comparison test in **b-g.** *p < 0.05, **p < 0.01, ***p < 0.001 and ****p < 000.1

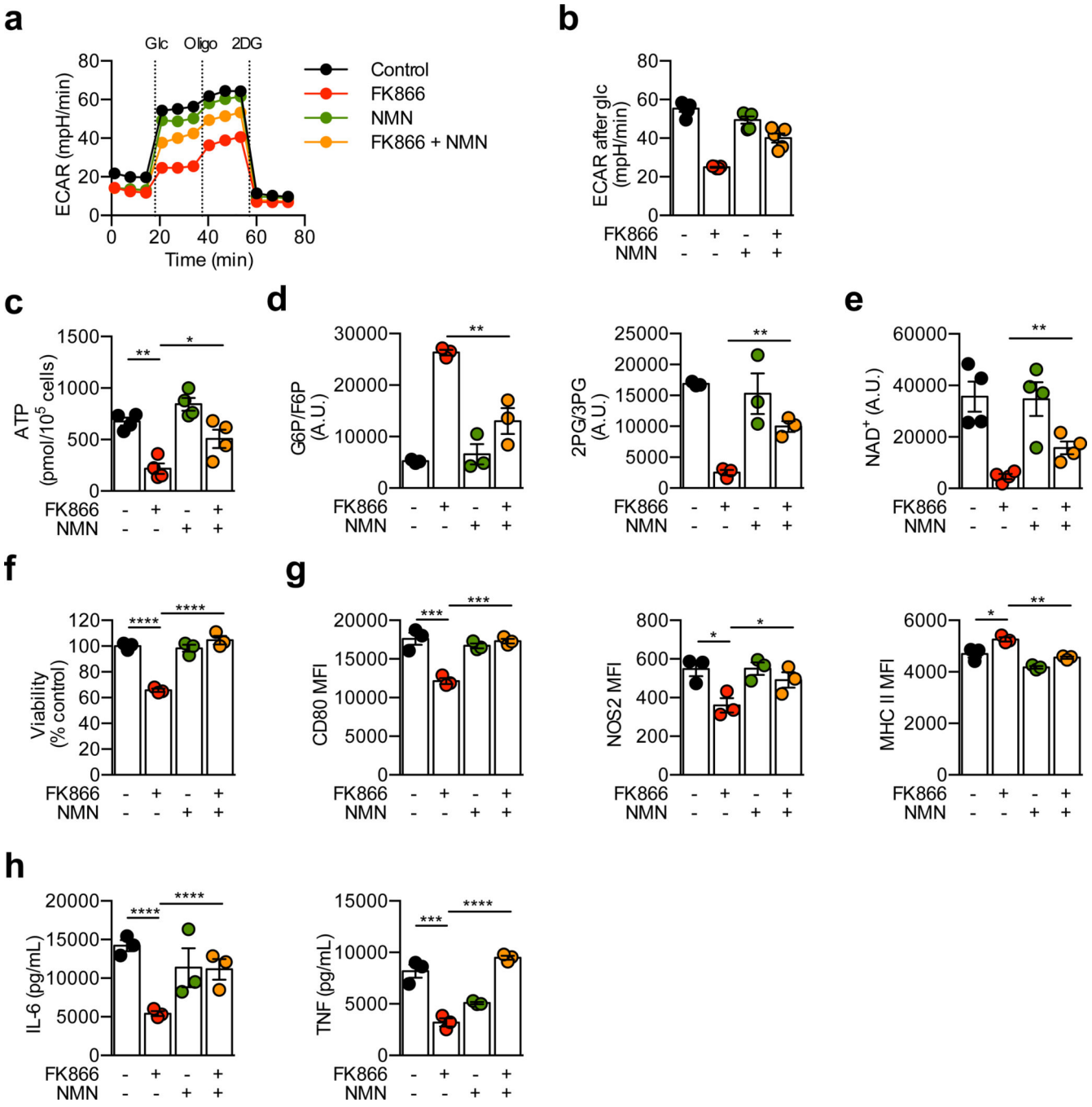

Figure 5: Nicotinamide mononucleotide addition rescues the inhibitory effects of NAMPT loss of function on inflammatory macrophage activation.

(**a-d**) M(γ+LPS) were polarized in the presence of vehicle control or treated with 50 nM FK866, 1 mM NMN or both FK and NMN for 18 h. (**a**) Real-time changes in the ECAR measured using Seahorse (n = 5 technical replicates, representative of five independent experiments). (**b**) ECAR after glucose injection (n = 5 technical replicates, representative of five independent experiments. (**c**) ATP quantification (n = 4 biologically independent samples, representative of three independent experiments). (**d**) Glycolytic intermediates

G6P/F6P and 2PG/3PG as measured by LCMS (*n* = 3 biologically independent samples, representative of three independent experiments). (**e**) NAD^+ in M(γ+LPS) untreated or treated with 50 nM FK866, 1 mM NMN or both FK and NMN for 8 h as quantified by LCMS (*n* = 3 biologically independent samples, representative of four independent experiments). Viability (**g**) and expression of markers CD80 (**h**), NOS2 (**i**) and MHC II (**j**) or cytokines IL-6 (**k**) or TNF (**l**) in M(γ+LPS) with or without FK866, NMN or both FK and NMN treatment for 18 h, analyzed by flow cytometry (**g-j**) or ELISA (**k,l**) (*n* = 3 biologically independent samples, data are representative of three (**k, l**) or four (**g-j**) independent experiments). Error bars are mean ± SEM. Data were analyzed by one-way ANOVA with Tukey's multiple comparison test.*p < 0.05, **p < 0.01, ***p < 0.001 and ****p < 000.1

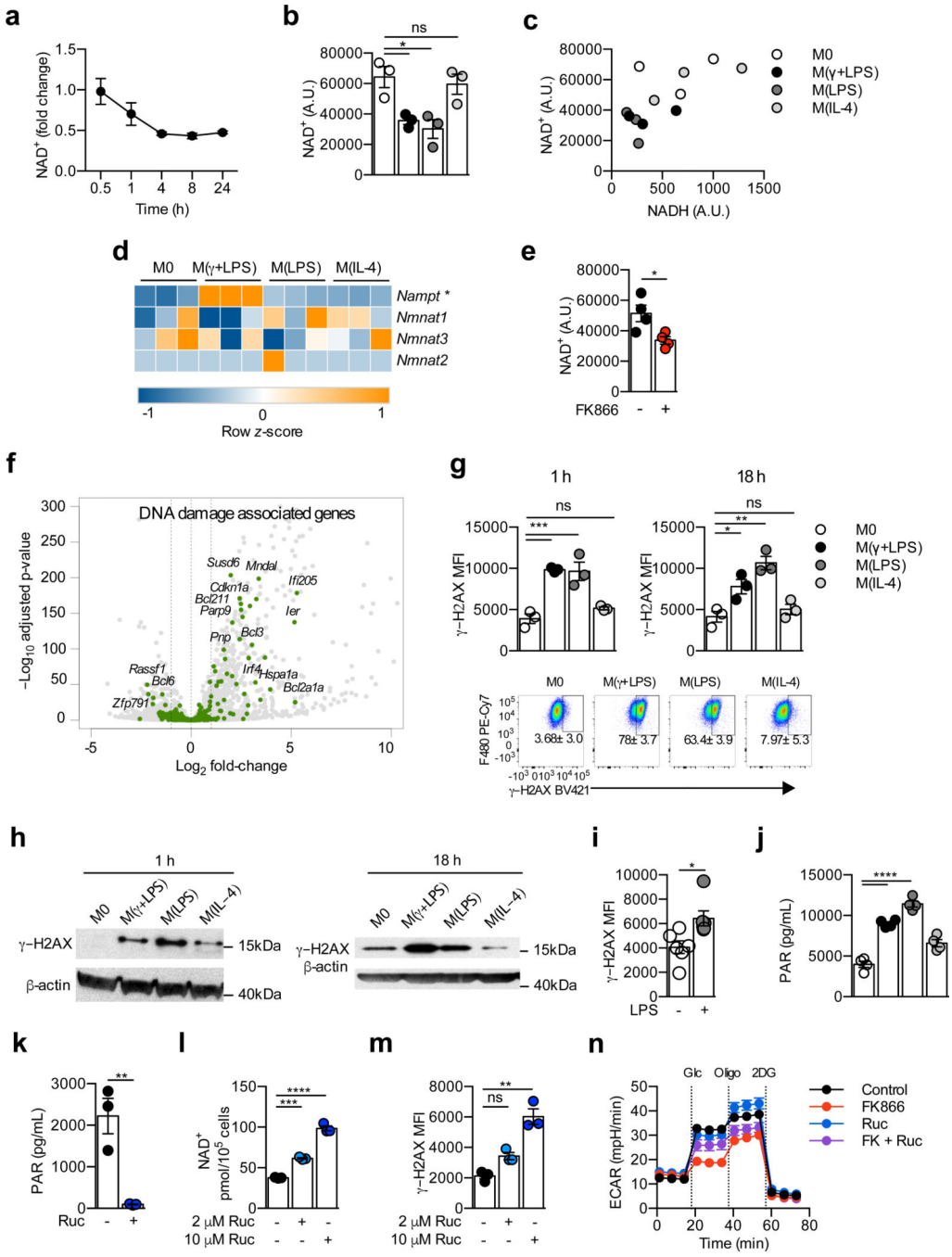

Figure 6: γ/LPS exposure induces rapid NAD$^+$ depletion and DNA damage accumulation.

(**a**) NAD$^+$ measurements over time during M(γ+LPS) polarization, presented relative to M0, and NAD$^+$ (**b**) and NAD$^+$ and NADH (**c**) in M0, M(γ+LPS), M(LPS) and M(IL-4) polarized for 1 h, as measured by LCMS (n = 3 biologically independent samples, representative of three (**b,c**) or five (**a**) independent experiments). (**d**) Heatmap of NAD$^+$ salvage gene expression in M0, M(γ+LPS), M(LPS) and M(IL-4) polarized for 1 h. Statistically significant (adjusted p value < 0.1) up- or down-regulated (>2 fold) genes denoted by * in M(γ+LPS) compared to M0 (n = 3 biologically independent samples).

(**e**) NAD^+ of M(γ+LPS) control or FK866 treated cells polarized for 1 h, as measured by LC-MS (*n* = 4 biologically independent samples, representative of three independent experiments). (**f**) Volcano plot showing expression of genes annotated with the Gene Ontology term "cellular response to DNA damage stimulus**"** based on RNA-seq data. Genes highlighted are significantly upregulated in M(γ+LPS) compared to M0 after 1 h of polarization (*n* = 3 biologically independent samples). (**g**) γ−H2AX staining in macrophages polarized as indicated, and representative flow cytomtery plots with indicated percentage of γ−$H2AX^+$ cells and SEM (*n* =. 3 biologically independent samples, representative of over ten independent experiments). (**h**) Immunoblot analysis of γ−H2AX in M0, M(γ+LPS), M(LPS) and M(IL-4) after 1 h or 18 h of culture. The blot was cropped to show relevant bands, and is representative of three independent experiments with similar results. (**i**) γ−H2AX expression in pMacs isolated from mice 1 h after delivery of i.p. PBS or LPS (*n* = 6 mice, representative of two independent experiments). PAR activity of (**j**) M0, M(γ+LPS), M(LPS) and M(IL-4) and (**k**) M(γ+LPS) with 10 μM Ruc or vehicle control, polarized for 1h (*n* = 4 (**j**), *n* = 3 (**k**) biologically independent samples, data are representative of three independent experiments). (**l,m**) M(γ+LPS) were polarized with 2 or 10 μM Ruc, (**l**) after 18 h NAD^+ as quantified by cycling assay and (**m**) after 4 h γ−H2AX expression analysed by flow cytometry (*n* = 3 biologically independent samples, representative of three independent experiments). (**n**) Real time changes in the ECAR of M(γ+LPS) polarized with or without 50 nM FK866, 10 μM Ruc or both inhibitors combined (*n* = 6 technical replicates, data are representative of five independent experiments). Error bars are mean ± SEM. Data were analyzed by one-way ANOVA with Tukey's multiple comparison test (**b, e, g, j, l, m**) or by unpaired, two-sided Student's *t*-test (**e, i, k**). *p < 0.05, **p < 0.01, ***p < 0.001 and ****p < 000.1).

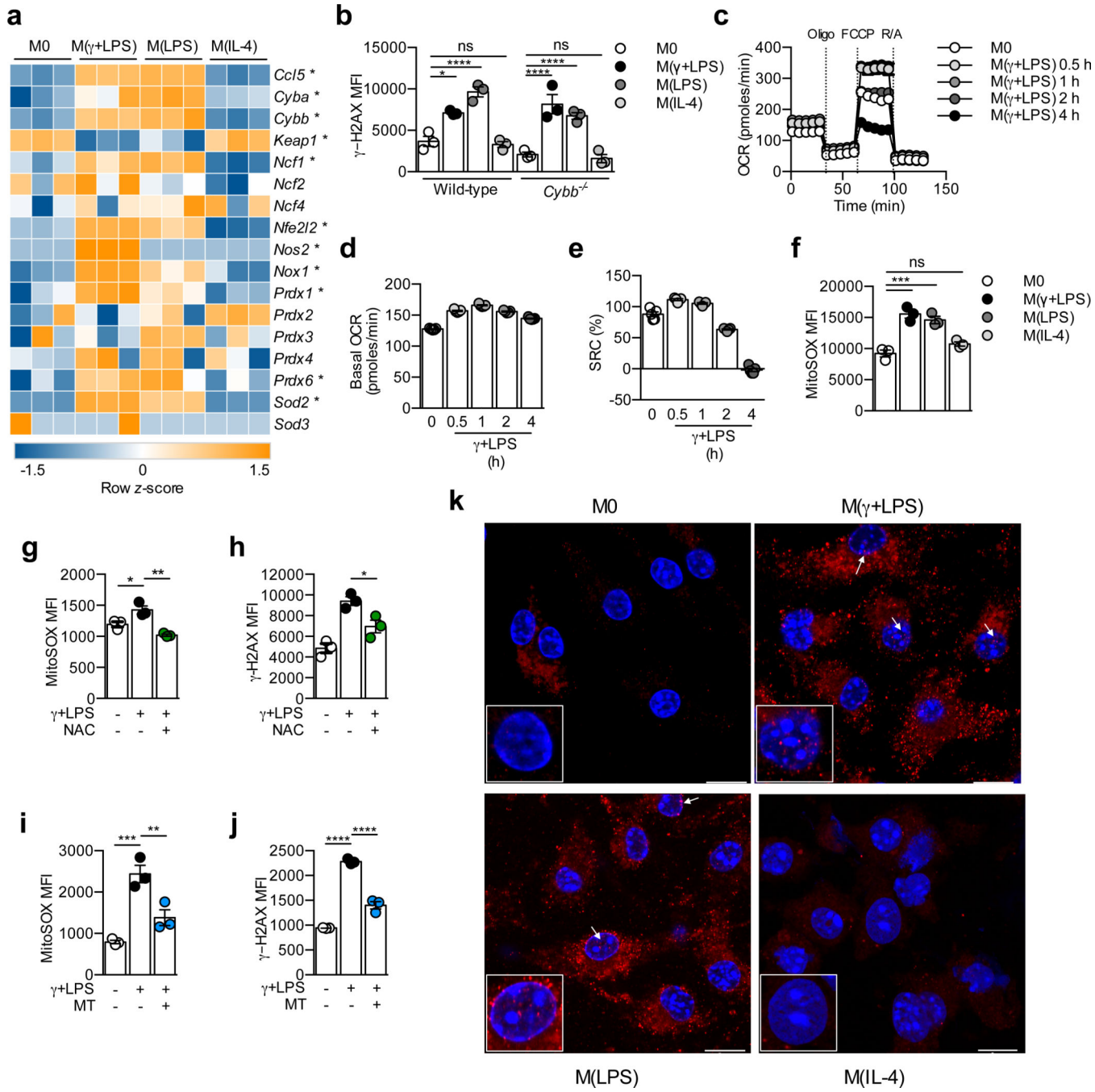

Figure 7: γ+LPS-induced mitochondrial ROS drives oxidative DNA damage

(**a**) Heatmap of genes expressed in response to ROS production and oxidative stress from of RNA-seq data of 1h polarized M0, M(γ+LPS), M(LPS) and M(IL-4). Statistically significant (adjusted p value < 0.1) up or down-regulated (> 2 fold) genes denoted by * in M(γ+LPS) polarized cells compared to M0 (*n* = 3 biologically independent samples). (**b**) γ−H2AX expression in wild-type or *Cybb*$^{-/-}$ macrophages polarized for 1 h as indicated (*n* = 3 biologically independent samples, representative of three independent experiments). Real time changes in OCR (**c**), basal OCR (**d**) and SRC (**e**) of macrophages unstimulated, or

stimulated with γ+LPS for 0.5–4 h as indicated (*n* = five technical replicates, representative of three independent experiments). (**f**) Flow cytometric analysis of MitoSOX staining in M0, M(γ+LPS), M(LPS) and M(IL-4) polarized for 1 h (*n* = 3 biologically independent samples, representative of over ten independent experiments). Macrophages were treated with 10 mM n-acetylscysteine (NAC; **g, h**) or MitoTempol (MT; **i, j**) for 1 h, and subsequently left unpolarized (M0), or polarized with γ+LPS and MitoSox staining (**g, i**) and γ−H2AX expression (**h, j**) were assessed by flow cytometry (*n* = 3 biologically independent samples, representative of four independent experiments). (**k**) 8-oxo-DG staining assessed by confocal microscopy in M0, M(γ+LPS), M(LPS) and M(IL-4) polarized for 1 h. Scale bar: 5 μm, white arrows indicate nuclear co-localization of 8OHG staining, insert shows an enlargement of nuclei with 8OHG staining (data are representative of three independent experiments. Each experiment was performed with 3 biologically independent samples with 10 images collected per sample, per condition). Error bars are mean ± SEM. Data were analyzed by one-way ANOVA with Tukey's multiple comparison test. *p < 0.05, **p < 0.01, ***p < 0.001 and ****p < 000.1.

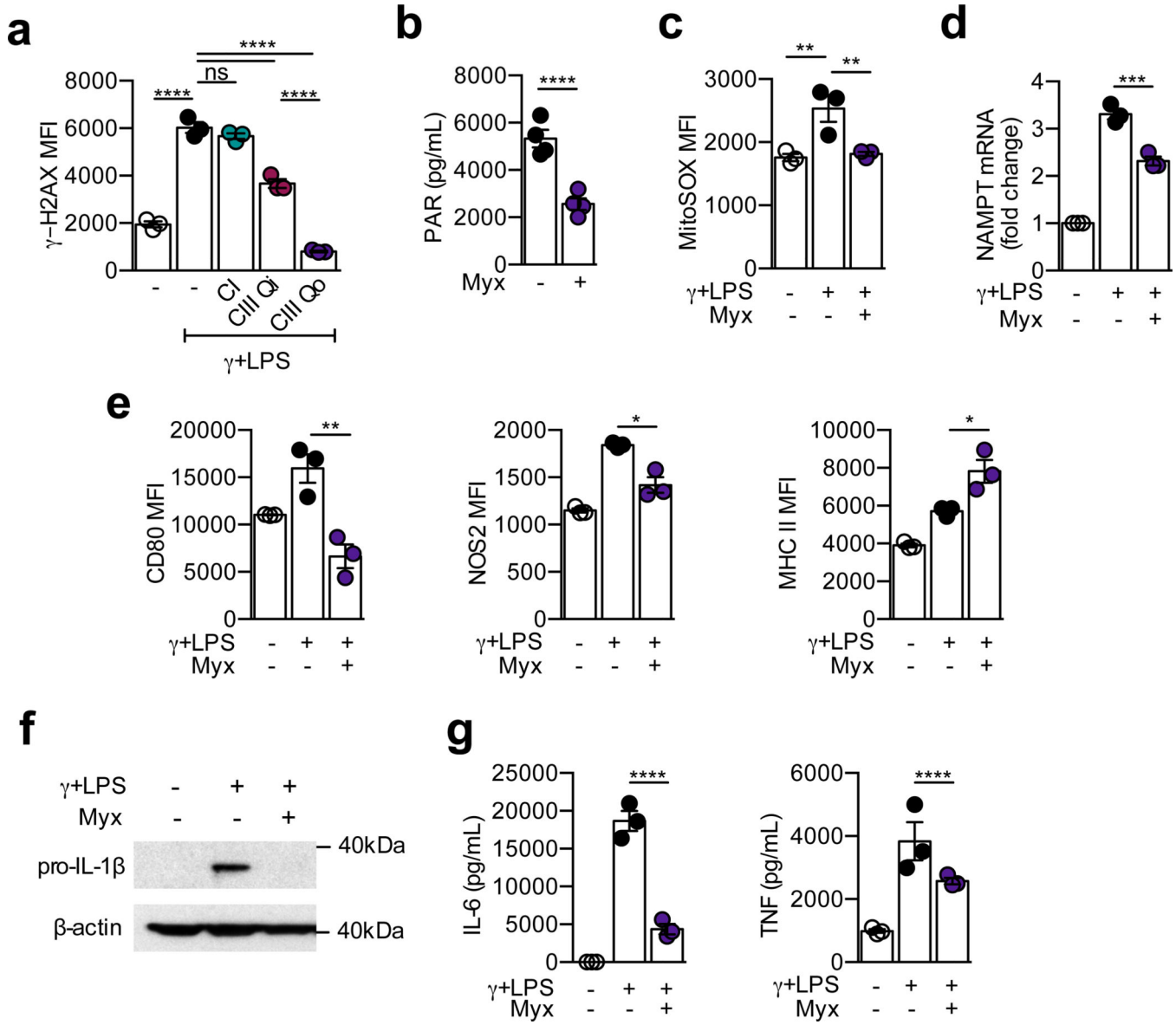

Figure 8: Mitochondrial ROS is produced by Complex III and required for inflammatory macrophage polarization.

In panels **a-d**; macrophages were pre-treated for 1 h with inhibitors then stimulated with γ+LPS, and 1 h later harvested. (**a**) γ−H2AX staining in M0 or M(γ+LPS) untreated or treated with the Complex I inhibitor rotenone (CI), a Complex III Qi inhibitor antimycin (CIII Qi) or a a Complex III Qo inhibitor myxothiazole (Myx; CIII Qo) (*n* = 3 biologically independent samples, representative of five independent experiments). (**b**) PAR quantification in 1h polarized M(γ+LPS) untreated or treated with myx (*n* = 4 biologically independent samples, representative of two independent experiments). (**c**) MitoSox staining in M0 or M(γ+LPS) untreated or treated with myx) (*n* = 3 biologically independent samples, representative of three independent experiments). (**d**) Expression of NAMPT mRNA in macrophages polarized as indicated for 1 h, normalized to mRNA encoding HPRT and presented relative to M0 control cells, set as 1 (*n* = 3 biologically independent

samples, representative of two independent experiments). In panels **e**-**g**; macrophages were pre-treated for 1 h with Myx then stimulated with γ+LPS, 1 h later cells were washed and fresh γ+LPS added. After 18 h cells were analysed. (**e**) CD80, NOS2 and MHC II expression was assessed by flow cytometry ($n = 3$ biologically independent samples, representative of three independent experiments). (**f**) Pro-IL-1β was assayed by immunoblot, the blot was cropped to show relevant bands, and is representative of three independent experiments with similar results. (**g**) IL-6 and TNF production detected by ELISA ($n = 3$ biologically independent samples, representative of three independent experiments). Error bars are mean ± SEM. Data were analyzed by one-way ANOVA with Tukey's multiple comparison test, with the exception of panel **b**, which was analyzed by unpaired, two-sided Student's *t*-test. *p < 0.05, **p < 0.01, ***p < 0.001 and ****p < 000.1.